Proceedings of the ASME 2015 International Design Engineering Technical Conferences & Computers and Information in Engineering Conference
IDETC/CIE 2015
August 2-5, 2015, Boston, Massachusetts, USA

DETC2015-48024

TENSILE PROPERTIES OF INKJET 3D PRINTED PARTS: CRITICAL PROCESS PARAMETERS AND THEIR EFFICIENT ANALYSIS

Jochen Mueller*
Engineering Design and Computing Laboratory
Department of Mechanical and Process Engineering
ETH Zurich
8091 Zurich, Switzerland
Email: jm@ethz.ch

Shi En Kim
Department of Mechanical and Civil Engineering
California Institute of Technology
Pasadena, CA 91125, USA
Email: shi_en_kim@caltech.edu

Kristina Shea
Engineering Design and Computing Laboratory
Department of Mechanical and Process Engineering
ETH Zurich
8091 Zurich, Switzerland
Email: kshea@ethz.ch

Chiara Daraio
Materials by Design and Nonlinear Dynamics
Department of Mechanical and Process Engineering
ETH Zurich
8091 Zurich, Switzerland
Email: daraio@ethz.ch

ABSTRACT

To design and optimize for capabilities of additive manufacturing processes it is also necessary to understand and model their variations in geometric and mechanical properties. In this paper, such variations of inkjet 3D printed parts are systematically investigated by analyzing parameters of the whole process, i.e. storage of the material, printing, testing, and storage of finished parts. The goal is to both understand the process and determine the parameters that lead to the best mechanical properties and the most accurate geometric properties. Using models based on this understanding, we can design and optimize parts, and fabricate and test them successfully, thus closing the loop. Since AM materials change rapidly and this process will have to be repeated, it is shown how to create a cost and time efficient experimental design with the one-factor-at-a-time and design of experiments methods, yielding high statistical accuracies for both main and interaction effects. The results show that the number of intersections between layers and nozzles along the load-direction has the strongest impact on the mechanical properties followed by the UV exposure time, which is investigated by part spacing, the position on the printing table and the expiry date of the material. Minor effects are found for the storage time and the surface roughness is not affected by any factor. Nozzle blockage, which leads to a smaller flow-rate of printing material, significantly affected the width and waviness of the printed product. Furthermore, the machine's warm-up time is found to be an important factor.

1 INTRODUCTION

Variations over a wide range of structural properties of Additively Manufactured (AM) parts are among the main issues designers face when designing and optimizing products for AM. Material-structure-process interactions often yield highly anisotropic materials which are hard to model, but which need to be taken into account when creating optimized mechanical structures fabricated with AM. The large diversity between current printing processes and materials adds to the complexity and highlights the need for a sophisticated and systematic test method. At the same time, recent multi-material printers increase the complexity even further by introducing additional process parameters and ranges of materials used in one printing process. Further, due to the fact that the suppliers are constantly changing and improving such materials, the testing process needs to be repeated and thus efficient.

To put this paper into context, a Design for Additive Manufacturing (DfAM) product design cycle, e.g. for designing an

*Address all correspondence to this author.

optimized helmet for AM, is presented (Figure 1) and includes characterizing AM in terms of material, process and structural parameters as the first step, the subject of this paper. This is followed by developing quantitative and simulation models, optimizing designs using computational methods [1,2], and then fabricating and testing the final product. Once testing of the product is completed, refinement of quantitative models, can be carried out for future product design cycles. Conventional, static material data sheets and paper-based DfAM guidelines are not sufficient anymore as the properties of AM parts are dependent on the specific processes and topologies of the structures, which also determine the printability of the models. Hence, the database and models need to be updated continuously as part of the iterative process. As it can be seen, initial testing and AM characterization is a crucial first step to capitalize on the unique capabilities of the AM fabrication process.

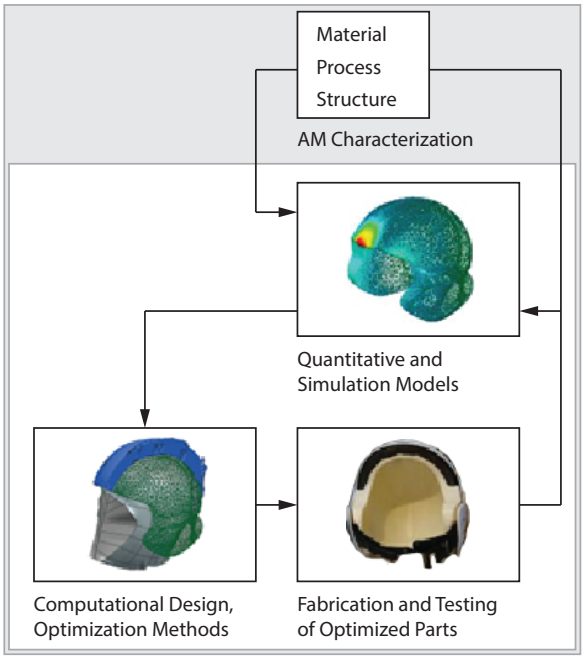

FIGURE 1: Conventional design process (white box) extended to the DfAM methodology for customized AM products.

The AM process investigated in this paper is inkjet 3D printing, which combines high spatial resolution with the ability to print multiple materials per tray. The ranges of material properties provided from the manufacturers are large, yet little is known about the impact of the process parameters on the printed material and structural properties. The current industrial focus of such a machine is still predominantly prototyping and printing of multi-color, rather than multi-material parts. Further, while systematic testing of metal AM processes is becoming more widespread [3], similar studies of polymer-based processes lags behind. One test method that meets these requirements is Design of Experiments (DoE), which is commonly used in industry and research [4]. However, its correct application is crucial for obtaining accurate and repeatable results and the actual analysis goes far beyond the simple application of a tool.

Therefore, in this work we show an efficient way of collecting relevant data with the DoE method and extensively analyze the complete process of inkjet 3D printing, ranging from the storage of model material over the printing process to the final part, with a focus on tensile properties. The paper is organized as follows. First, previous work examining the process capability of inkjet 3D printing is elaborated. It is followed by the experimental methods, which describe the investigated parameters, the statistical methods and the experimental set-up. The results are then presented and discussed based on their chronological importance and on how to ideally set the parameters to achieve the best possible results for designing parts for this AM technology.

2 BACKGROUND

In inkjet printing, liquidized photo-polymer is jetted onto a surface and instantly cured with UV-light. Standard printers contain at least two print heads, similar to the ones in conventional inkjet printing, with numerous linearly aligned nozzles. One print head is usually allocated to the model material and one to the support material. More print heads can be added for higher material throughputs or to print multiple materials, which is one major advantage of the process. Thin layers of cured material accumulate while the build tray slowly moves down until the part is finished [5].

In earlier works, Singh [6] investigated the geometric accuracies of parts fabricated on an Objet Eden 260, on which Kesy and Kotlinski [7] examined the influence of part orientation on mechanical strength and hardness. For transverse orientations in the X-Z-plane, the parts demonstrated a yield point, whereas for parts laying in the X-Y-plane, brittle rupture was dominant and reduced mechanical strength was observed. They attributed these properties to the UV exposure time.

The mechanical properties, dimensions and surface roughnesses of parts printed from different Vero-materials on an Objet Eden 330 were characterized by Pilipovi, Raos and Sercer [8]. Scale factors, which needed to be accounted for manually on that printer type, were optimized by Brajlih, Drstvensek, Kovacic and Balic [9]. In another experiment, Udroiu and Mihail [10] reported that Objet Eden 350's glossy option resulted in smoother surfaces compared to the mat option. Design rules were derived by Gibson et al. [11] who investigated the application of living hinges printed in the same model.

The Objet350 Connex, which can print up to three discrete materials at a time, was studied by Barclift and Williams [4]. Concentrating on in-process parameters, they examined the longitudinal orientation of the part on the printing table in X and Y direction, the transverse orientation in X, Y and Z direction as well as the part spacing for VeroWhite (FullCure 830) material – the directional definitions are according to the ASTM F2792-12a standard [12]. A significant impact was found only for the latter one, where a tight spacing yielded higher UV exposure time and thus stronger parts. They also pointed out the complexity and interrelation of impacting factors and demonstrated the need for a systematic approach.

However, many more factors with potential impact are available, including out-of-process parameters. Such an independent analysis has yet to be performed for the Objet500 Connex3, the

subject of this paper, which is one of the most advanced multi-material printers available on the market today [13]. Compared to the previously mentioned models, it allows combination of three different resins to print up to 82 materials per job in addition to the support material [14]. Stratasys also continuously improves their material formulations and meanwhile introduced a new VeroWhitePlus (Fullcure 835) material, which has not been tested in detail yet. This demonstrates the need for a systematic and efficient test method to enable design and optimization of parts for this AM process.

3 EXPERIMENTAL METHODS

The experimental methods cover the input parameters on which the statistical methods are based. Further, the fabrication and metrology is described.

3.1 Input factors

The input factors investigated in this work are identified from the mentioned literature and complemented with additional parameters found by analyzing the complete process described in "The Eight Steps in Additive Manufacturing" [15]. The set of six factors examined with DoE is presented in Table 1 and Figure 2 and explained as follows,

- The positions X and Y of the parts' center of gravity on the printing table, where the low and high levels represent the minimum and maximum reachable coordinates.
- The longitudinal and transverse directions depict the orientation of the parts. The longitudinal direction is either X or Y. Due to the slim shape of the specimens, the Z direction needs to be investigated separately using support structure. The levels of the transverse direction are dependent on the longitudinal direction. When the longitudinal direction is parallel to X, the low level of the transverse direction is Y and vice versa, indicating that the part is aligned horizontally in the X-Y plane. The transverse direction in Z is defined as the high level.
- Part-spacing is taken to be an indirect measure of UV intensity. Since each test specimen is printed in an individual printing job, two additional specimens are added in both the X and Y direction, but not part of the analysis. The minima and maxima are chosen depending on the table size.
- Two batches of materials with different expiry dates one year apart (denoted as 2014 and 2015, which represents their approximate, overall serviceable life as defined by Objet) are examined.

More potentially impacting parameters are identified, but are costly and/or time-consuming to manipulate and hence not suitable for the DoE analysis. Knowledge of them, however, is important to draw educated conclusions from the tests and reduce testing time during the actual DoE tests. The following parameters are therefore investigated beforehand using the one-factor-at-a-time (OFAT) approach, where one factor is investigated while all other factors are kept constant.

- Warm-up time of the machine: First, a batch of specimens is printed on the cold machine, followed by a random job of ten hours to fully warm up the machine, before the second batch is printed on the warm machine.
- Cleanliness of the print heads' nozzles: Material can cure not just in the layers, but also on the print-head, which leads to blockage of nozzles. Therefore, for the warm state previously described, it is distinguished between clean and not clean, where the print-head is either cleaned between the prints or not. In each job, three parts are printed. This is repeated twice, totaling a sample size of nine per setting and 27 overall. All runs are randomized.
- Time between printing and testing: To test the effect of aging on tensile properties, a period of 21 days is scheduled with decreasing intervals between tests. That leads to specimens being stored for 21, 17, 13, 9, 6, 3, 1 and 0 days before testing. The storage conditions are kept constant and recorded over the whole period. Ten specimens are printed per tray, oriented longitudinally and transversely in the Y and Z direction, respectively. The part spacing is fixed at 10 mm.
- Storage in support material: The support material is removed from five out of the ten parts described previously. The other five parts are stored inside the support material. For the analysis, the means of each group are taken based on a pairwise comparison, so that the samples are always compared to other ones with identical settings.

As for the material, VeroWhitePlus (RGD835) is used and the remaining material cartridge slots of the printer are filled with TangoBlack+, VeroYellow and SUP705, a combination of which the support structure is built. Factors not of interest, but with po-

TABLE 1: Fractional factorial design factors with corresponding maximum and minimum levels. The unit of the numbers in the upper part is millimeters.

Factor	Name	Level (low)	Level (high)
A	Position (X)	41.75	448.25
B	Position (Y)	41.75	348.25
C	Longitudinal dir.	X	Y
D	Transverse dir.	X/Y	Z
E	Part spacing (X)	10	343
F	Part spacing (Y)	10	243
Block	**Expiry date material**		
1	2014		
2	2015		

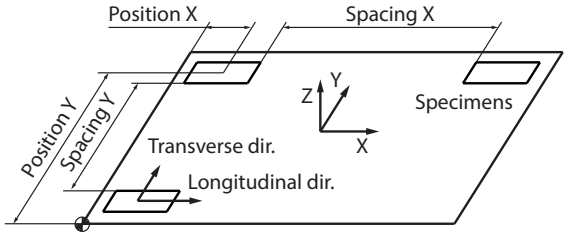

FIGURE 2: Printing table indicating the directions, orientations and part spacings of the fabricated specimens. Shown is the test-specimen (upper-left corner) plus the two specimens added for part spacings.

tential influence on the result, are kept constant for all tests. They include the printing mode, e.g. high quality versus digital material, support material composition, environmental conditions of storage for both raw materials and test-specimens, printing and testing, i.e. temperature, relative humidity and UV exposure.

3.2 Statistical method

DoE is a statistical approach in which the levels of multiple factors are changed at the same time, rather than investigating them one-by-one as it is done in the OFAT approach. Factors are process parameters, e.g. distance between parts, and levels are their associated settings, e.g. 10 mm and 243 mm. To increase the accuracy and reduce the effect of noise, the levels are chosen in the maximum possible distance. In the analysis of the results, each factor, or combination of factors, is taken individually and the means of each level is calculated. The differences between the means are called effects and are analyzed for its statistical significance with the Analysis of Variance (ANOVA) methods. The DoE can compensate for random error sources and higher statistical accuracies can be achieved compared to conventional methods. Also, by comparing combinations of factors instead of individual factors, the interaction effects between different factors can be found. Interaction effects are described in levels, where the number of levels depicts the amount of compared factors for the interaction. For instance, a *level 2 interaction effect* compares two factors and tells that a response of factor A is significant only when factor B is set at a certain level or vice versa. That also means that main effects are included in interaction effects and that low-order interaction effects are included in high-order interaction effects. DoE provides a table outlining the run order of the test runs with the respective configuration of the factors. Ideally, all known factors which are not part of the DoE are kept constant throughout the tests, e.g. layer thickness. Since some factors are not controllable, e.g. humidity, the run order is randomized to prevent systematic errors. If a factor is of interest, but not trivial to change, for instance switching the material between the two batches, blocks can be integrated. The factors are then randomized only within the blocks [16].

It is in the nature of such analyses that not all investigated factors are of relevance, which is why it is recommended that a screening design is performed in the first step. In a screening design, all factors are investigated roughly with a poor statistical accuracy, only to find out which ones are of relevance. In the next step, the relevant factors are taken, a new design is created and experiments are repeated. To decrease the overall number of tests, in the following paragraphs we show how to skip the initial screening design by making reasonable assumptions while maintaining full statistical accuracy. This procedure is also shown as an example for the set-up used in this work in Figure 3.

1. Since main and low-order interaction effects are part of high-order effects, knowledge of the latter ones is more important. Interactions of level 4 and above are highly unlikely [17]. Hence, a half fractional factorial design is chosen, which is a specific type of DoE that reduces the number of tests by 50% compared to testing all the possible combinations of factors and levels and that is able to map interaction effects up to level 3.

2. Statistically insignificant factors, which will not influence the results if their levels are changed, can be removed from the design. Repeating the ANOVA, the accuracy increases due to (relatively) smaller residuals. Removing one factor from a half fractional factorial design yields a full factorial design, which analyzes all possible combinations of factors and levels, and not just the ones up to level 3. Removing two or more factors replicates the full factorial design, meaning that each configuration is tested multiple times and therefore increasing the statistical accuracy.

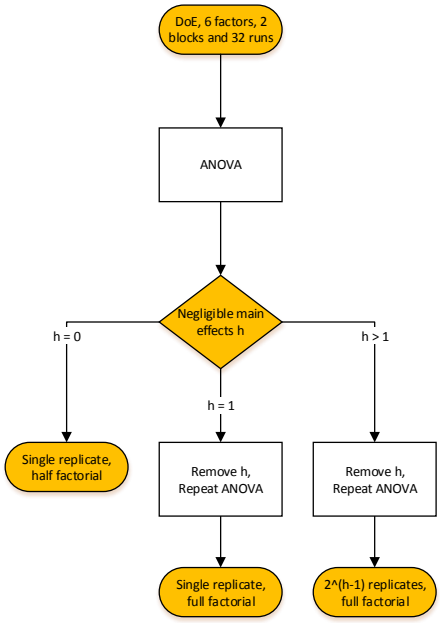

FIGURE 3: DoE sub-process indicating the effects of the reduction of the number of main factors.

For the analysis, the ANOVA tables provide information on the variances within groups (residuals mean square, MS_{res}) and between groups of treatment conditions (treatment mean squares, MS_{treat}). The mean squares are the ratios of the sum of squares (SS_{res}, SS_{treat}) and their adjacent degrees of freedom (df). Based on MS_{res}/MS_{treat}, the F ratio is calculated, which shows potential impact of the treatment groups when $F > 1$. The value of P, obtained from the F value, is a measure of the validity of the null hypothesis (a standard significance level of $\alpha = 0.05$ is chosen) and indicates the likelihood that a value lies within the range provided. [16].

3.3 Fabrication and removal of support material

All specimens are printed on a Stratasys Objet500 Connex3 in an air-conditioned room. The printer contains eight parallel print heads, six of which are allocated to three different materials i.e. two per material. Each print head consists of 96 linearly aligned nozzles, measuring 50 μm in diameter. Unless otherwise stated, the support material is removed from the specimens mechanically. This procedure, rather than using the water jet process, prevents the absorption of water into the structure, potentially changing the results. Further, this step removed the need for adding drying and dehydration time prior to testing. For parts

on which the surface roughness and waviness are measured, the effect of water absorption is negligible compared to mechanical surface damage, which is why a high-pressure water jet is used to clean those specimens (Krumm RK 5 XL VA). Since blocked nozzles can yield a rough surface finish which, in turns, can alter the spreading behavior of the liquid polymer [18], the print heads are cleaned before each run.

3.4 Tensile testing

The elastic modulus (E), ultimate tensile strength (UTS) and Poisson's ratio (ν) are measured and post-processed in accordance to the ASTM D638-10 standard [19]. To stay within the vertical travel length of the printer for longitudinal alignment in Z, Type IV specimen geometry is chosen and used for all tests for comparability. The measurements are taken using an Instron ElectroPuls E3000 in combination with a Dynacell load cell of 5 kN load capacity (linearity and repeatability better than $\pm 0.25\%$ in the tested range). A constant testing speed of 50 mm/min is used for all tests.

3.5 Geometry and mass measurements

The dimensions and surface roughness are measured with a Mitutoyo Micrometer Series 102 (accuracy of $\pm 2\ \mu m$) and a Perthen perthometer M4P, respectively. Five measurements are taken on different areas and averaged. For the waviness, a standard micrometer with *extra slim* grippers is used. The mass is measured with a Metler Toledo XS205 DualRange scale (linearity of ± 0.2 mg, repeatability of 0.01 mg).

4 RESULTS

Results are presented for all parameters studied in this section starting with the OFAT and then the DOE.

4.1 Warm-up time and cleanliness of nozzles

At $\alpha = 5\%$, the warm up of the machine (comparing room temperature RT to warm/clean, Table 2) has no statistical significance on all of the properties except on the width of the cross section and the mass, for which the difference between the means is 0.21% and 1.14%, respectively. However, nozzle blockage (RT to warm/not clean) is significant especially for the geometric properties, i.e. the length (0.05%), specimen mass (5.14%), maximum thickness (-10.44%), and thus, the maximum deviation from the thickness (766.55%). Of all the mechanical properties, only the elongation of break is affected (17.38%). Further, it is observed that the standard deviation increases when the nozzles are not cleaned.

4.2 Time between printing and testing with different storage conditions

The measured mean temperature in the storage room was 21.84 ^{o}C (0.62), the humidity was 48.73 % (1.89) and no UV exposure was present. Despite the relatively small standard deviations, the results did not display any clear trends for all mechanical properties tested (Figure 4). However, for the ultimate tensile strength, slightly higher values are observed for parts stored without support material and an opposite effect is observed for Young's modulus.

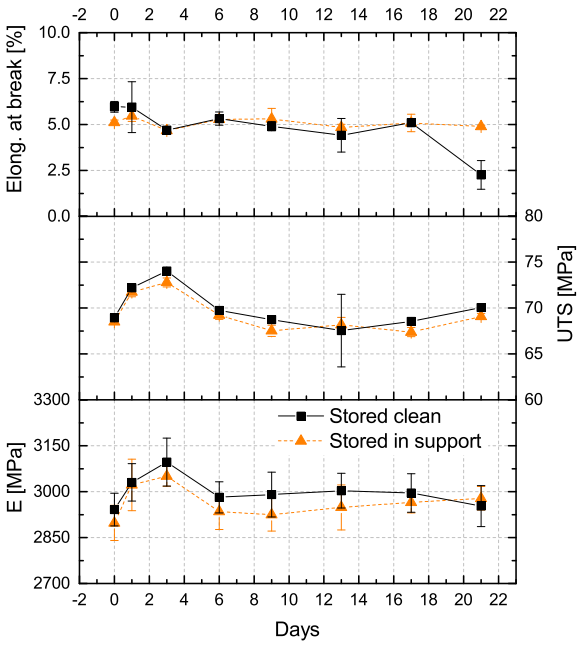

FIGURE 4: Aging effect on Young's modulus (bottom), ultimate tensile strength (center) and elongation at break (top). The symbols depict the means of five tests each, and the bars the standard deviation.

For the mass, an increasing trend is observed with increasing storage time (Figure 5). While the maximum mean of the mass after 21 days is at 1.7602 g for the clean and 1.7818 g for the part stored in the support structure, respectively, both of them are about 2.5% higher than at shorter storage times. A t-test, conducted on the maximum and minimum values, compares two different treatments on factors to determine whether there is a real difference between the means by providing a significance level p. The traditional threshold for statistical significance is $p = 5\%$ [20] and used throughout this work. The results show p-values of 2.607e-06, 8.005e-08, 3.697e-06, 2.015e-04 (for inside support, 21 versus 0 days/without support, 21 versus 0 days, respectively), hence statistical relevance is confirmed. Further, it is observed that the discrepancy between parts free of support material and parts inside support material increases with time.

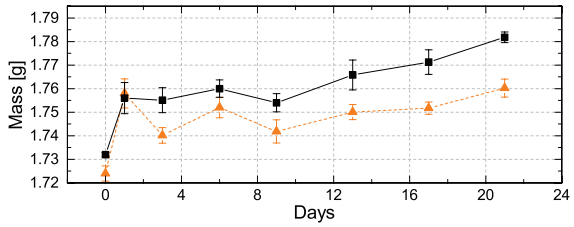

FIGURE 5: Aging effect on mass. The symbols depict the means of five tests each, the bars the standard deviation.

4.3 Design of Experiments test

The analysis of the level 3 interaction effects of the 6 factors and 2 blocks revealed no significance for Young's modulus,

TABLE 2: Impact on properties due to a cold machine ('RT') versus warm machine. For the latter case, in one test series the nozzles are cleaned ('Warm/clean'), while they are left as they are after the previous print in the other test series ('Warm/not clean').

	RT	Warm/clean			Warm/not clean		
	Mean (s.d.)	Mean (s.d.)	t	p	Mean (s.d.)	t	p
Length (L0) [mm]	63.43 (0.02)	63.42 (0.02)	1.35	0.195	63.40 (0.02)	3.37	0.004
Width (W0) [mm]	9.51 (0.02)	9.53 (0.02)	-2.06	0.056	9.50 (0.01)	1.62	0.137
Width cross section (Wc) [mm]	3.12 (0.02)	3.14 (0.02)	-3.36	0.007	3.11 (0.01)	1.25	0.230
Thickness (T) [mm]	3.16 (0.01)	3.16 (0.01)	-1.11	0.286	2.83 (0.10)	9.64	<0.001
Mass [g]	1.75 (0.01)	1.77 (0.01)	-6.57	<0.001	1.66 (0.02)	10.35	<0.001
Young's modulus [MPa]	2924 (44)	2922 (76)	0.08	0.941	2984 (113)	-1.48	0.169
Ultimate tensile strength [MPa]	67.30 (1.57)	69.03 (1.15)	-2.67	0.018	68.13 (2.68)	-0.80	0.438
Rupture strain [%]	5.35 (0.34)	5.70 (0.99)	-1.00	0.342	4.42 (0.44)	5.04	<0.001
Ra (top) [m]	3.37 (0.45)	3.26 (0.46)	0.51	0.614	4.17 (1.36)	-1.67	0.127
Rz (top) [m]	16.45 (2.08)	16.09 (2.14)	0.36	0.727	18.34 (6.32)	-0.86	0.413
Rmax (top) [m]	20.92 (4.25)	20.73 (2.36)	0.12	0.910	31.49 (13.10)	-2.30	0.045
Max. deviation from thickness [μm]	26.67 (8.66)	27.78 (8.33)	-0.28	0.785	231.11 (91.03)	-6.71	<0.001

ultimate tensile strength and elongation at break. Therefore, it is conducted on main and level 2 interaction effects only. The ANOVA table is shown in Table 3.

No significant impacts on Young's modulus are found for either main effects or level 2 interaction effects, which are denoted by "*". For ultimate tensile strength, the factors involved in significant level 2 interactions are A*E (p = 0.019), C*D (p = 0.014) and C*F (p = 0.042). B is irrelevant for both, main and level 2 interaction effects and thus deleted. The new design, analyzed based on 5 factors, results in a 2^5 full factorial design. No significant interactions are found for 5th, 4th and 3rd order, hence the analysis is reduced to level 2 interactions. The results are shown in Table 4.

TABLE 4: ANOVA table of ultimate tensile strength effects for the 2^5 full factorial design after taking out the Y position factor. A: Position X, C/D: Longitudinal/transverse dir., E/F: Part spacing X/Y.

Source	df	SS	MS	F	p
Blocks	1	184.45	184.45	144.59	<0.001
A	1	5.15	5.15	4.04	0.063
C	1	6.22	6.22	4.88	0.043
D	1	76.34	76.34	59.84	<0.001
E	1	2.20	2.20	1.72	0.209
F	1	40.12	40.12	31.45	<0.001
A*C	1	2.22	2.22	1.74	0.207
A*D	1	1.81	1.81	1.42	0.252
A*E	1	9.66	9.66	7.57	0.015
A*F	1	1.92	1.92	1.50	0.239
C*D	1	10.93	10.93	8.57	0.010
C*E	1	0.73	0.73	0.58	0.460
C*F	1	6.66	6.66	5.22	0.037
D*E	1	0.66	0.66	0.52	0.484
D*F	1	0.01	0.01	0.01	0.920
E*F	1	0.16	0.16	0.12	0.731
Error	15	19.13	1.28		
Total	31	368.35			

Compared to the full ANOVA, the p values decreased for all interactions: A*E (p = 0.015), C*D (p = 0.010) and C*F (p = 0.037). As all relevant main effects are part of them, only the interaction effects are shown (Figure 6). With few exceptions, the low levels of A, C, E and F provide higher output values, whereas the opposite is true for D. The strongest effect originates from D, where the mean of the vertical direction is 4.41% higher than the horizontally oriented one. In F, the difference between high and low is 3.68%, and for all others it is as low as 1.5%. The highest values result from a combination of high D and low F.

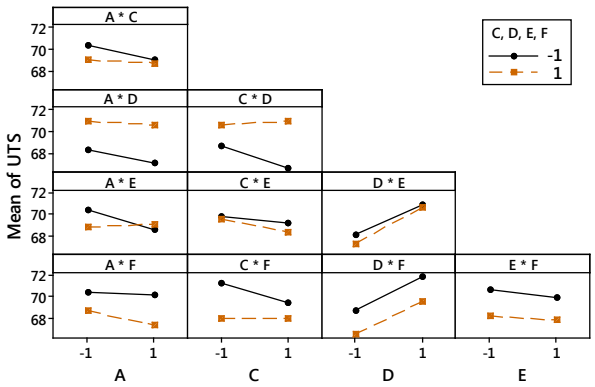

FIGURE 6: Interaction plots for ultimate tensile strength. The legend refers to the second values of the compared interaction. A: Position X, C/D: Longitudinal/transverse dir., E/F: Part spacing X/Y.

Significant impacts on elongation at break originate from A*C (p = 0.007), C*D (p = 0.004), C*E (p = 0.007) and D*E (p = 0.002). As before, B, but also F do not play a significant role for either of the effects and are therefore excluded, which yields a full factorial design with two replications. Repeating the ANOVA, the new results shown in Table 5 are calculated. The effects are still the same, but with p values decreasing to 0.001 or smaller, the statistical accuracy is even higher: A*C (p = 0.001), C*D (p = 0.001), C*E (p = 0.001) and D*E (p = <0.001). Again, all main effects are included and thus not investigated separately.

When examining the interaction plots for A, the low levels yield a shorter elongation at break for all combinations. For C, D and E a higher elongation at break is reached with the only exception being the high level of E in combination with D (Figure 7). The largest effect is found for C, with a maximum difference

TABLE 3: Full ANOVA table of Youngs's modulus, ultimate tensile strength and elongation at break. A/B: Position X/Y, C/D: Longitudinal/transverse dir., E/F: Part spacing X/Y.

	Young's modulus					Ultimate tensile strength				Elongation at break			
Source	**df**	**SS**	**MS**	**F**	**p**	**SS**	**MS**	**F**	**p**	**SS**	**MS**	**F**	**p**
Blocks	1	49905	49904.80	7.78	0.021	184.45	184.45	155.97	<0.001	11.67	11.67	19.87	0.002
A	1	765	765.30	0.12	0.738	5.15	5.15	4.35	0.067	6.95	6.95	11.83	0.007
B	1	4407	4407.30	0.69	0.429	5.00	5.00	4.23	0.070	0.83	0.83	1.41	0.265
C	1	1629	1629.10	0.25	0.626	6.22	6.22	5.26	0.047	40.68	40.68	69.30	<0.001
D	1	9772	9772.10	1.52	0.248	76.34	76.34	64.55	<0.001	6.17	6.17	10.51	0.010
E	1	3315	3314.60	0.52	0.490	2.20	2.20	1.86	0.206	4.53	4.53	7.72	0.021
F	1	5852	5852.40	0.91	0.364	40.12	40.12	33.92	<0.001	0.01	0.01	0.02	0.880
A*B	1	6599	6599.30	1.03	0.337	0.08	0.08	0.07	0.804	0.03	0.03	0.04	0.839
A*C	1	13217	13217.10	2.06	0.185	2.22	2.22	1.88	0.204	7.06	7.06	12.03	0.007
A*D	1	2	2.40	<0.01	0.985	1.81	1.81	1.53	0.247	1.42	1.42	2.42	0.154
A*E	1	40	39.70	0.01	0.939	9.66	9.66	8.17	0.019	0.08	0.08	0.14	0.714
A*F	1	155	155.30	0.02	0.880	1.92	1.92	1.62	0.235	0.42	0.41	0.71	0.422
B*C	1	<1	<0.01	<0.01	1.000	<0.01	<0.01	<0.01	1.000	<0.01	<0.01	<0.01	1.000
B*D	1	43	43.00	0.01	0.937	0.32	0.32	0.27	0.613	<0.01	<0.01	0.01	0.942
B*E	1	768	767.60	0.12	0.737	1.73	1.73	1.46	0.257	1.27	1.27	2.16	0.176
B*F	1	2598	2598.30	0.41	0.540	1.36	1.36	1.15	0.312	0.52	0.51	0.88	0.373
C*D	1	3119	3119.40	0.49	0.503	10.93	10.93	9.24	0.014	8.62	8.62	14.68	0.004
C*E	1	8482	8481.90	1.32	0.280	0.73	0.73	0.62	0.451	7.25	7.25	12.35	0.007
C*F	1	328	328.30	0.05	0.826	6.66	6.66	5.63	0.042	0.78	0.78	1.32	0.280
D*E	1	29	28.90	<0.01	0.948	0.66	0.66	0.56	0.475	10.09	10.09	17.19	0.002
D*F	1	3212	3211.70	0.50	0.497	0.01	0.01	0.01	0.918	0.03	0.03	0.05	0.834
E*F	1	29	28.90	<0.01	0.948	0.16	0.16	0.13	0.724	0.88	0.88	1.50	0.251
Error	9	57708	6412.00			10.64	1.18			5.28	0.59		
Total	31	171975				368.35				114.56			

TABLE 5: ANOVA table for elongation of break, 2^4 full factorial design with 2 replicates after taking out B and F. A: Position X, C/D: Longitudinal/transverse dir., E: Part spacing X.

Source	**df**	**SS**	**MS**	**F**	**p**
Blocks	1	11.69	11.69	23.25	<0.001
A	1	6.94	6.94	13.80	0.001
C	1	40.73	40.73	81.00	<0.001
D	1	6.18	6.18	12.29	0.002
E	1	4.55	4.55	9.04	0.007
A*C	1	7.09	7.09	14.10	0.001
A*D	1	1.42	1.42	2.82	0.108
A*E	1	0.08	0.08	0.16	0.691
C*D	1	8.59	8.59	17.09	0.001
C*E	1	7.28	7.28	14.47	0.001
D*E	1	10.06	10.06	20.00	<0.001
Error	20	10.06	0.50		
Total	31	114.64			

of more than 30% between the means of X and Y orientation followed by factors A and D with differences close to 15%.

The numerical values of all factor's means and standard deviations are given in Table 6.

Between the blocks of different material expiry dates, p-values far below 5% are reached. This indicates that the effects of the blocks are statistically significant for all of the mechanical properties (Table 7). It also shows that, within a year of raw-material storage, the Young's modulus decreases by 79 MPA (2.79% based on the lower value), the ultimate tensile strength by

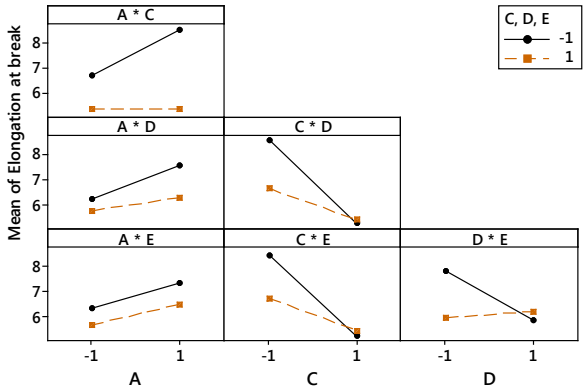

FIGURE 7: Interaction plots for elongation at break. The legend refers to the second values of the compared interaction. A: Position X, C/D: Longitudinal/transverse dir., E: Part spacing X.

4.8 MPa (7.18%) and the elongation at break by 1.21% (20.58%).

All ANOVAs conducted in this section are checked for model adequacy using normal probability plots of residuals, versus fits and histograms. Nothing significant is revealed for any tests.

4.4 Longitudinal direction in Z

Since the values of the measurements of longitudinal Z orientation are compared to all other values measured in the X/Y plane, which are not normally distributed, the previously used t-test does not suit. Instead, the Mann-Whitney-Wilcoxon test, which does not require a normal distribution of the compared populations, is used. Compared to the t-test has a smaller statis-

TABLE 6: Mean values of the levels of the factors tested in the DoE. A/B: Position X/Y, C/D: Longitudinal/transverse dir., E/F: Part spacing X/Y.

Factor	Level	Mean (s.d.) E [MPa]	UTS [MPa]	EAB [%]
A	41.75	2873 (108)	69.62 (3.29)	6.02 (1.25)
	448.25	2863 (96)	68.82 (4.36)	6.95 (2.37)
B	41.75	2880 (101)	69.61 (3.87)	6.32 (1.98)
	348.25	2856 (103)	68.82 (3.86)	6.64 (1.92)
C	X	2861 (99)	69.66 (3.52)	7.61 (2.18)
	Y	2875 (106)	68.78 (4.17)	5.36 (0.44)
D	X/Y	2850 (97)	67.67 (3.62)	6.92 (2.56)
	Z	2885 (105)	70.76 (3.46)	6.04 (0.82)
E	10	2878 (97)	69.48 (3.38)	6.86 (2.52)
	343	2858 (107)	68.96 (4.32)	6.11 (1.00)
F	10	2881 (86)	70.34 (3.71)	6.46 (1.79)
	243	2854 (115)	68.10 (3.71)	6.50 (2.11)

TABLE 7: F-test and p results for blocks for Young's modulus (E), ultimate tensile strength (UTS) and elongation at break.

	Block	Mean (s.d.)	F	p
E [MPa]	2014	2828 (65)	12.43	0.002
	2015	2907 (63)		
UTS [MPa]	2014	66.82 (2.65)	90.55	<0.001
	2015	71.62 (2.29)		
EAB [%]	2014	7.09 (2.48)	6.40	0.018
	2015	5.88 (0.86)		

tical power, but allows to compare the results to the other results, regardless of the effects of other factors. Significant differences are found for Young's modulus (7.93% weaker), ultimate tensile strength (40.61% weaker), and elongation at break (72.54% shorter)(Table 8).

TABLE 8: Mann-Whitney-Wilcoxon test results for longitudinal alignment along X/Y versus Z directions

	Mean (X/Y)	Mean (Z)	W	p
E [MPa]	2918.15	2686.82	380	<0.001
UTS [MPa]	69.05	41.01	384	<0.001
EAB [%]	7.10	1.95	384	<0.001

5 DISCUSSION

For VeroWhitePlus, Objet provides data for the elastic modulus of 2000-3000 MPa, tensile strength of 50-65 MPa and elongation at break of 10-25% [5]. On average the tested elastic moduli found are close to the upper limit, whereas the ultimate tensile strength exceeds the listed value by more than 5 MPa in several tests. For elongation at break, however, the results are considerably lower than the ranges provided by Objet. Due to the fact that other Objet machines and settings were used in previous research, these values cannot be compared directly. Barclift and Williams generally observed lower output values, but, despite not always statistically significant, similar trends are reported here, i.e. longitudinal alignments along X, transverse orientation along Z and tight part spacing provided, on average, the highest strengths and moduli.

5.1 Warm-up time and cleanliness of nozzles

RT - warm/clean: While the printer is running, friction affected parts heat up and so does the printing table from the UV lights. When warm material from the nozzles touches the surface, there is a gradient in temperature yielding different thermal contractions. Therefore, the YX printing orientation potentially leads to an increase in the cross sectional width Wc. The increase in width W is not statistically significant, but shows the same trend. Overall, the resulting, larger surface area absorbs more moisture from the air, potentially leading to the larger mass observed.

RT - warm/not clean: Blocked nozzles result in a smaller flow rate, which, in turn, can decrease the length, thickness and thus the mass of the specimens. Since not all nozzles were blocked and due to the longitudinal specimen orientation along X, the machine was still able to produce the same lengths. The smaller rupture strain can be explained by both the increased surface roughness and the deviation from the shape (i.e. waviness), leading to higher stress concentrations.

5.2 Time between printing and testing with different storage conditions

Despite a sample size of 5 per property, no clear trend is discovered for the mechanical properties. Since all specimens are printed and measured in one run, unwanted, systematic errors could not be excluded. However, the same constant conditions as for all other tests are used so that it can be concluded, that the effect of aging is relatively small compared to other impacting factors. For deeper insight, replicated experiments need to be conducted with an appropriate sample size. Concerning the mass, the moisture resistance property of plastics indicate the sensitivity of such materials to humidity in surrounding air, which explains the weight gain of the samples with increasing storage time. When the samples are cooled down to room temperature in a relatively short period, the effect increases. The increasing gap between clean storage and storage in support material indicates that the support material slows down the absorption process.

5.3 Expiry date of the material

The aging effect is mentioned, but not quantified, by Gibson, Rosen and Stucker [15]. In accordance, in our tests, a statistically meaningful impact is found for Young's modulus, ultimate tensile strength and elongation at break. As the material becomes stronger and stiffer, the compliance (i.e. elongation at break) decreases. While it is hard to determine whether the reason is the aging of the material or changes in the material formulation, it can be said that Objet seems to continuously improve their material properties (compare VeroWhite from 2009 with VeroWhitePlus from 2014 [5]).

5.4 Design of Experiments test

No significance is found for the Young's modulus in the DoE-tested factors. The higher standard deviations possibly arise from the additional post-processing step, where a curve is fitted to the experimental data for finding the initial slope of the curve. The size of the residuals increases to 25% of the total sum of squares, leading to a decreased F ratio – an indication that an impact on Young's modulus exists but is not found.

For the ultimate tensile strength, statistically significant effects are found for all factors except for the position in Y, which is, however, close to the 5%. As the idle position of the print head is in the X(min) and Y(max) corner, two effects are possible: a) the machine is optimized for this position with respect to the strength of the guides and b) specimens close to this position receive more UV light than the ones further away because the print head moves back to the X-origin for all movements in Y-direction (Figure 8). This also heats up the table more at this position, leading to the effect described previously.

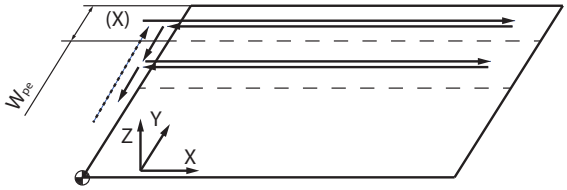

FIGURE 8: Effective width (w_{pe}) and moving path of the print head. (X) indicates the idle position of the head.

In the longitudinal alignment X, fewer nozzles are used compared to Y orientation, yielding a smaller number of intersections between material depositions within the layers; compare Figures 9a and 9b to Figures 9c and 9d. It can be seen, within the layers, indicated with orange/shaded color, XY and XZ have longer, but fewer lines than YX and YZ. Further, the intersections in this orientation are aligned along the direction of the applied load of the tensile tests. When the length of the specimens is smaller than w_{pe}, the difference in exposure time to UV light is insignificant. For the transverse alignment, the vertical direction consists of more layers and thus more intersections, leading to an increased UV exposure time; as contrasted in Figures 9a and 9c (fewer layers), and Figures 9b and 9d (more layers). Because the mean number of intersections between layers and nozzles is identical, it is safe to assume that UV light is the major factor in this case. The part spacing in X only plays a minor role, which is possibly due to the movement of the printing head: it moves back and forth only in X, regardless of how much surface is covered in material within that path. Therefore, the exposure time remains about the same, even though the time difference between the back and forth movement is slightly bigger for the larger distance. For part spacing Y, the nozzle length w_{pe} is not able to cover the full length of both specimens in one run (Figure 8). Thus, the print head moves twice at almost the same position exposing those areas to more UV light. As hypothesized, this leads to a positive effect on the mechanical properties of parts longitudinally oriented along Y; for the X orientation, the head only moves once, resulting in lower values.

The ascending curve of the position X for elongation at break is opposite to the stiffness and strength curves. An opposite effect is also observed for the longitudinal orientation. Since both of these settings experience increased UV exposure time, it is assumed that UV light hardens the material, which has a negative effect on the elongation at break. The longitudinal alignment and the spacing in X show similar, downward trends with respect to the strength values. Both experienced identical exposure times,

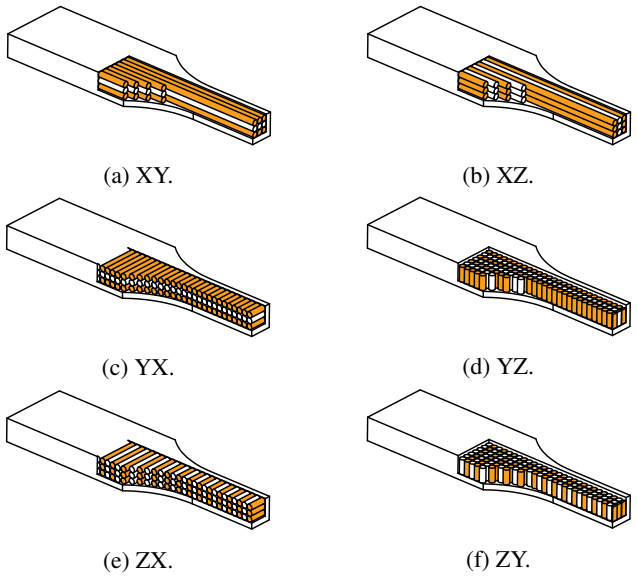

FIGURE 9: Test specimens indicating the print directions (cylinders) and layers (shading of the cylinders) for the different print orientations. The first symbol indicates the longitudinal direction on the printing table and the second one the transverse direction.

confirming that the strengthening mechanisms described before seem to apply to the elongation at break too.

5.5 Longitudinal direction in Z

Due to the larger number of vertical layers (Figures 9e and 9f), printing in vertical direction takes longer compared to other orientations, leading to the highest UV exposure time. However, higher numbers of layers also yield higher numbers of intersections. As the mechanical properties are considerably lower for parts aligned along Z compared to all other orientations, it can be concluded that the weakening effect of more layers is greater than the strengthening effect of increased UV exposure. However, the influence of the support structure for the vertical prints cannot be fully excluded from the results.

5.6 Implications for testing, design and optimization

The one-factor-at-a-time method is used to preliminarily test for the out-of-process parameters that are potentially time-saving in the main (in-process) tests. The method revealed that a cold machine produced similar mechanical, but not geometric properties as with a warm machine. To maintain a high geometric accuracy, cleaning the print head after each job is crucial. For achieving comparable results, it is also important to keep the time between printing and testing constant, and to remove the support structure after printing, as the parts' mass and mechanical properties change with time.

To investigate the in-process parameters, Design of Experiments is chosen to drastically reduce the testing time compared to conventional methods. A modification of the initial design allowed for the study of even the high order interaction effects and increased the statistical accuracy further. The best combination of the factor's levels in terms of stiffness and strength is found to be for parts printed close to the point of X/Y origin. Regarding the applied load direction, an alignment parallel to the X axis is

preferable, followed by an alignment parallel to the Y axis. As the material decays with time, the newest production date shall be used and when printing multiple parts in one tray, they should be arranged closely. To increase the elongation at break, generally speaking, the opposite recommendations are true.

The standard deviations are relatively small and so are the residuals in the ANOVA, indicating that all major impact factors are found. It illustrates that, in controlled environments, accurate and reproducible results can be achieved. This knowledge and accurate material data of the anisotropic behavior of such structures will assist designers who are interested in not only the prints' visual aspects, but also in the mechanical performance and optimization.

6 CONCLUSION

This paper investigates variations of inkjet 3D printed parts in terms of both tensile and geometric properties by analyzing parameters of the whole AM process to determine the best conditions under which to fabricate. The goal of this understanding is to enable the design and optimization of functional parts, as opposed to the current focus on prototypes for this process. All major impact factors influencing the parts' properties are identified and quantified and best practice is given for achieving the best mechanical and geometric properties. Accurate results with small standard deviations are reached when printing under controlled conditions. It is also shown that, by carefully selecting and defining the test order and method, an efficient experimental design can be created from existing methods that is applicable to other AM processes.

ACKNOWLEDGMENT

This research is supported by the ETH Zurich, Seed Project SP-MaP 02-14, "Additive Manufacturing of Complex-Shaped Parts with Locally Tunable Materials".

REFERENCES

[1] Stankovic, T., Mueller, J., Egan, P., and Shea, K., 2015. "Optimization of additively manufactured multi-material lattice structures using generalized optimality criteria". In ASME 2015 International Design Engineering Technical Conferences and Computers and Information in Engineering Conference (IDETC/CIE 2015), ASME.

[2] Stankovic, T., Mueller, J., Egan, P., and Shea, K., 2015. "A generalized optimality criteria method for optimization of additively manufactured multi-material lattice structures". *Journal of Mechanical Design, Special issue on "Design for Additive Manufacturing'*.

[3] F3122-14, A., 2014. *Standard Guide for Evaluating Mechanical Properties of Metal Materials Made via Additive Manufacturing Processes*. West Conshohocken, PA.

[4] Barclift, M., and Williams, C., 2012. "Examining variability in the mechanical properties of parts manufactured via polyjet direct 3d printing". *International Solid Freeform Fabrication Symposium, Austin, TX*.

[5] Stratasys, 2014. Professional 3d-printing - stratasys. `http://www.stratasys.com`. Accessed: 2015-01-23.

[6] Singh, R., 2011. "Process capability study of polyjet printing for plastic components". *Journal of Mechanical Science and Technology,* ***25***(4), pp. 1011–1015.

[7] Kesy, A., and Kotlinski, J., 2010. "Mechanical properties of parts produces by using polymer jetting technology". *Archives of Civil and Mechanical Engineering,* ***X***(3).

[8] Pilipovi, A., Raos, P., and Sercer, M., 2009. "Experimental analysis of properties of materials for rapid prototyping". *The International Journal of Advanced Manufacturing Technology,* ***40***(1-2), pp. 105–115.

[9] Brajlih, T., Drstvensek, I., Kovacic, M., and Balic, J., 2006. "Optimizing scale factors of the polyjet rapid prototyping procedure by genetic programming". *Journal of achievements in materials and manufacturing engineering,* ***16***(1-2), May-June, pp. 101–106. Special Issue of CAM3S'2005.

[10] Udroiu, R., and Mihail, L. A., 2009. "Experimental determination of surface roughness of parts obtained by rapid prototyping". In Proceedings of the 8th ICECS, WSEAS.

[11] Gibson, I., Goenka, G., Narasimhan, R., and Bhat, N., 2010. "Design rules for additive manufacture". *Proceedings of the SFF 2010,* ***16***, pp. 705–716. University of Texas, Austin, Texas.

[12] F2792-12a, A., 2012. *Standard Terminology for Additive Manufacturing Technologies*. West Conshohocken, PA.

[13] Alphacam, 2014. Kunststoffspritzformen aus dem 3d drucker. `http://www.alphacam.de/dynamic/ksf/Praesentation_PolyJet_Form.pdf`. Accessed: 2014-12-03.

[14] Stratasys, 2014. Connex3 3d production systems - hundreds of materials for maximum versatility. `http://www.stratasys.com/3d-printers/production-series/connex3-systems`. Accessed: 2015-01-23.

[15] Gibson, I., Rosen, D., and Stucker, B., 2009. *Additive Manufacturing Technologies: Rapid Prototyping to Direct Digital Manufacturing*. Springer.

[16] Montgomery, D., 2012. *Design and Analysis of Experiments, 8th Edition*. John Wiley & Sons, Incorporated.

[17] Li, X., Sudarsanam, N., and Frey, D. D., 2006. "Regularities in data from factorial experiments". *Complexity,* ***11***(5).

[18] Mueller, J., Haghparastmojaveri, N., Alan, T., and Neild, A., 2013. "The role height plays in the spreading of liquid droplets over sharp edges". *Applied Physics Letters,* ***102***(4), p. 041605.

[19] D638-10, A., 2010. *Standard Test Method for Tensile Properties of Plastics*. West Conshohocken, PA.

[20] Nuzzo, R., 2014. "Statistical errors". *Nature,* ***506 (7874)***, p. 150.